Cement and Concrete Research 122 (2019) 251–256

Contents lists available at ScienceDirect

Cement and Concrete Research

journal homepage: www.elsevier.com/locate/cemconres

Quantification of NO_x uptake in plain and TiO_2-doped cementitious materials

Q. Jin[a], E.M. Saad[b], W. Zhang[a], Y. Tang[a,b], K.E. Kurtis[a,*]

[a] School of Civil and Environmental Engineering, Georgia Institute of Technology, Atlanta, GA, USA
[b] School of Earth and Atmospheric Sciences, Georgia Institute of Technology, Atlanta, GA, USA

ARTICLE INFO

Keywords:
TiO_2
NO_x photodegradation
Cement
Microstructure
Nitrite/Nitrate

ABSTRACT

This study brings new understanding of the interaction of nitrogen oxides (NO_x) with cement-based materials, necessary for optimizing these materials for NO_x sequestration. The masses of nitrites and nitrates produced through NO_x uptake in cement-based materials are quantified for both plain portland cement pastes (OPC) and nano TiO_2-doped OPC. Both nitrite and nitrate were bound within plain OPC, with a nitrite:nitrate ratio of 1:2. This intrinsic NO_x sequestration capacity is attributed to the microstructural features and alkalinity of cement-based materials. The capacity is increased by 360%, with a lower nitrite:nitrate ratio of 1:1.3, in TiO_2-doped OPC. The increase in NO_x uptake and the change in nitrite:nitrate ratio is attributed to the microstructural differences and activation of photocatalytic reactions that are associated with TiO_2 addition. Comparing NO_x exposure with and without UV on TiO_2-doped OPC shows that photocatalytic activities have greater influences on NO_x uptake than microstructural differences induced by TiO_2 addition.

1. Introduction

Nitrogen oxide (NO_x) emission is one of the most hazardous air pollutions, causing a variety of health problems such as respiratory system impairment and vision problems. NO_x also contributes to global warming, acid rain, ground-level smog, and decreased water quality [1,2]. The two most common forms of NO_x in the troposphere are nitric oxide (NO) and nitrogen dioxide (NO_2). NO is directly emitted from high temperature combustion, in particular from combustion engines in motor vehicles. NO_2 is produced from the interaction of NO with ozone or molecular oxygen [3,4]. Decades-long efforts to reduce NO_x levels have been mainly devoted to environmental legislation, improvements in combustion efficiency, and technologies to reduce post-combustion NO_x [5,6].

Among different technologies for reducing atmospheric NO_x, titanium dioxide (TiO_2) photocatalysts [7,8] have been of great interest. Since concrete is a widely used material globally, substantial efforts have been dedicated toward understanding its potential roles in NO_x binding through the introduction of photocatalysts. For example, paving with concrete containing or coated with TiO_2 nanoparticle photocatalysts [9,10] has been shown to reduce the amount of motor vehicle emission-derived NO_x in the air [11–13]. Given the ubiquity of concrete infrastructure, interest in expanding the applications of cement-based materials, such as to concrete bridges and buildings, is growing.

Previous research has mainly focused on the manner of photocatalyst addition (i.e., interblended vs. coatings) and their percent addition in cementitious substrates [14–16]. In these applications, both anatase and rutile TiO_2 nanoparticles have been shown to effectively remove NO_x from the atmosphere in the presence of water, oxygen, and UV light [17,18]. Studies have investigated the effects of microstructure and surface features on the photocatalytic performance of TiO_2 nanoparticles blended cementitious materials [19,20]. Studies also examine the effects of mixing and operation conditions on photocatalytic efficiency [21–23], and the feasibility of using alternative cementitious materials in combination with TiO_2 nanoparticles [24,25]. Yet, despite the considerable efforts in the above areas, a fundamental understanding of the speciation and fate of sequestered NO_x in the cementitious materials remains elusive.

In general, photocatalysis is believed to result in the oxidation of NO_x by hydroxyl radicals ($OH\cdot$) and superoxide radicals ($O_2\cdot^-$). This leads to the formation of nitrite (NO_2^-) and/or nitrate (NO_3^-) through a series of photocatalytic oxidation reactions [26–30], which can be generalized through the following equations:

$$TiO_2 \xrightarrow{h\nu} TiO_2 + e^- + h^+ \quad (1)$$

$$h^+ + H_2O \rightarrow H^+ + OH^\cdot \quad (2)$$

* Corresponding author.
E-mail address: kkurtis@gatech.edu (K.E. Kurtis).

https://doi.org/10.1016/j.cemconres.2019.05.010
Received 5 August 2018; Received in revised form 10 April 2019; Accepted 9 May 2019

$$e^- + O_2 \rightarrow O_2^{\bullet -} \quad (3)$$

$$NO + O_2^{\bullet -} \rightarrow NO_3^- \quad (4)$$

$$NO + OH^{\bullet} \rightarrow NO_2^- + H^+ \quad (5)$$

$$NO + OH^{\bullet} \rightarrow HNO_2 \quad (6)$$

$$HNO_2 + OH^{\bullet} \rightarrow NO_2 + H_2O \quad (7)$$

$$NO_2 + OH^{\bullet} \rightarrow NO_3^- + H^+ \quad (8)$$

However, the relative abundance of the produced nitrite and/or nitrate has not been clearly defined, and likely depends on the characteristics of the substrate material.

Because cement-based materials are structurally and chemically complex hydrated materials, they may influence and participate in these photocatalytic reactions, such as affecting the amount of nitrite and/or nitrate formed and the manner in which NO_x is bound within the material. Such information on N speciation and mass distribution is important for a number of reasons. First, due to the intrinsic chemical differences between nitrite and nitrate, they can interact differently with cementitious phases. For example, these ions could dissolve in the alkaline pore solution [31], adsorb to hydrate surfaces [31], and/or to substitute for sulfate ions within aluminum-bearing hydrated phases (AFm and AFt) [32]. Second, nitrite and nitrate, when incorporated into steel-reinforced concrete, can serve as corrosion inhibitors, with nitrates considered to be better inhibitors [33]. Recent studies have also shown that adjusting nitrite and nitrate concentrations to achieve a desirable ratio with chloride concentrations can enhance the corrosion resistance [34]. Therefore, information about the concentration and relative percentages of nitrite and nitrate formation is critical to understanding their interactions with the complex cementitious materials and to designing these materials for maximized NO_x uptake and corrosion resistance.

To quantify the concentration and relative percentages of nitrite and nitrate in TiO_2-doped cementitious materials after NO_x exposure, this study employs a novel experimental method combining wet chemical extraction, ultraviolet-visible (UV–vis) spectrophotometry, and ion chromatography (IC) measurements. While these approaches have been widely used in determining nitrite and nitrate concentration in other systems [35,36], this is the first time that these approaches have been used in cement-based materials. The NO_x sequestration capacity of various cementitious materials is determined through the measured nitrite and nitrate concentrations. The mass balance between the NO_x input and NO_x measured at the outlet is compared to measured nitrite and nitrate quantities in the exposed cement paste. Microstructural analysis is also carried out in this study to establish a relationship between microstructural features of cement-based materials with NO_x uptake.

2. Experiments and methods

2.1. Materials

The samples were prepared from ASTM C150 Type I/II ordinary portland cement (OPC, Argos, Atlanta, Georgia, USA), combined with 5 wt% TiO_2 (KRONOClean® 7050, Kronos Worldwide). The water-to-solid ratio was kept constant at 0.40. The chemical composition of the cement was obtained by oxide analysis (ASTM C114 [37]) and used to determine the Bogue composition (Table 1). The characteristics of the TiO_2 are listed in Table 2.

Table 1
Composition (wt%) and loss on ignition (LOI) of the cement.

C_3S	C_2S	C_3A	C_4AF	SiO_2	Al_2O_3	Fe_2O_3	CaO	MgO	SO_3	Na_2O	LOI
62.9	7.6	6.9	9.2	19.2	4.5	3	62.8	3.6	3.1	0.5	2.6

Table 2
Characteristics of TiO_2 photocatalyst (provided by manufacturer).

TiO_2 content	Phase	Density	Bulk density	Specific surface area
> 85%	Anatase	3.9 g/cm^3	300 g/L	> 225 m^2/g

To increase the surface area and the reaction potential between NO_x and the cementitious materials, crushed samples were produced from a cementitious plate. The plate was cast by first adding TiO_2 to deionized water (18.2 mΩ-cm) and mixing for 1 min using a handheld electric mixer to facilitate dispersion [31]. Then cement was added to the TiO_2 suspension and mixed for an additional 2 min. Cementitious plates were cast in plastic molds with dimension of 50.8 mm × 50.8 mm × 9.5 mm (width × length × height) and stored at 23 ± 2 °C under polyethylene sheeting to maintain a high humidity. After 24 h, the plates were removed from the molds and subsequently cured in limewater at room temperature (23 ± 2 °C) for 28 days. After curing, the plates were conditioned at 23 ± 2 °C and 50 ± 5% relative humidity until reaching constant mass (i.e., < 0.5 wt% change over a 6-h period). The crushed samples were obtained by hand crushing the conditioned plate and sieving to obtain particles which passed the No.18 (1 mm) and were retained on the No. 30 (0.6 mm) sieves. Samples were stored in double sealed plastic bags prior to the microstructural analysis and NO_x photodegradation tests to avoid drying or carbonation.

2.2. Microstructural analysis

The specific surface area (SSA) and pore size distribution of the crushed samples, prior to NO_x exposure, were determined by N_2 adsorption and desorption. Approximately 2 g of each sample were analyzed in a specific surface area gas analyzer (Micromeritics ASAP 2420) over a relative pressure range of 0.01 to 0.99. The crushed samples were degassed at 10 μmHg pressure for 12 h prior to the analysis. The SSA was determined by Brunauer–Emmett–Teller (BET) theory [38] using N_2 adsorption isotherm performed over a relative pressure range of 0.05 to 0.30. The pore size distribution was determined using Barrett, Joyner and Halenda (BJH) method [39] on the data obtained from the desorption isotherm [40].

Although it has been noted that surface area measurements vary with technique, adsorbate, and sample preparation [41], the variation due to the sample preparation was minimized in this study by using a consistent experimental method and procedure, as described above, facilitating comparison among samples. In addition, the N_2 adsorption and desorption technique for obtaining SSA and pore size distribution has been commonly used for cementitious materials and can ensure semiquantitative comparisons of different cementitious materials [42].

2.3. NO_x photodegradation

A schematic illustration of the NO_x photodegradation test setup is shown in Fig. 1. The test was performed following procedures in ISO 22197 [43] and JIS R 1701 Standards [44]. Two grams (2.00 ± 0.01 g) of samples were placed in a borosilicate photoreactor, with both ends sealed with a filter and screw cap. As recommended by the aforementioned standards, the NO_x gas used in this study was prepared by mixing 1000 ppb nitric oxide gas in ultrapure dry air and passed through the reactor at a constant flow rate of 1 L/min. For the purpose of consistency, the NO_x in this study refers to this particular mixed gas. The reaction was conducted at 23 ± 2 °C and 50 ± 5% relative humidity. The sample-loaded reactor was placed under two 40 W UV fluorescent lamps (Damar Worldwide) with peak emission at 365 nm. The UV light intensity at the sample surface was maintained at 10 W/m^2 by adjusting the distance between the UV light source and the samples, which reside on the bottom surface of the photoreactor. The initial gas concentration was kept at 1000 ppb before turning on the UV light. Once the gas

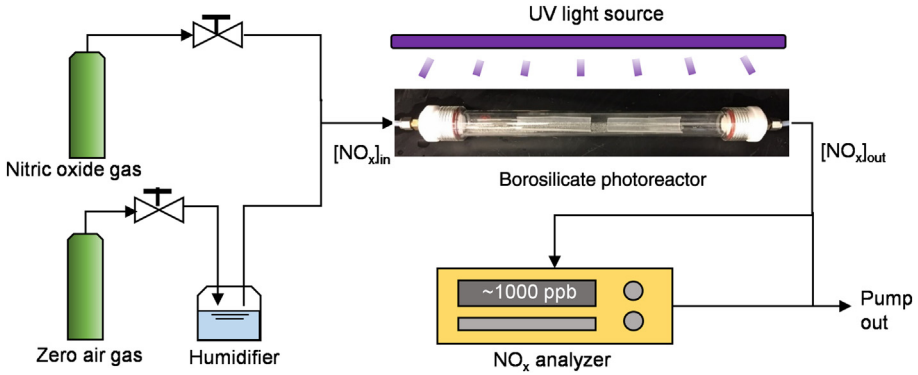

Fig. 1. Experimental setup for NO_x photocatalytic degradation test.

concentration stabilized (1 h stabilization time), the UV light exposure started and continued for 5 h. After the UV light was turned off, the gas concentration was allowed to re-stabilize for another hour. The gas concentration throughout the experiment was measured by a chemiluminescent $NO/NO_2/NO_x$ analyzer (Model 200A, Teledyne API). The entire test setup was covered by a black light-blocking canvas to prevent ambient light from affecting the reaction.

2.4. Sample matrix

Six groups of experiments were conducted in triplicate, with varied sample composition and reaction conditions. Sample labels, test matrix, material composition, and exposure conditions are summarized in Table 3. Samples PB, PB-N and PB-N-V were control groups prepared with plain OPC (i.e., no TiO_2 doping), and Samples PT, PT-N and PT-N-V contained 5% TiO_2 by weight of OPC. As outlined in Table 3, both doped and un-doped samples were subjected to three exposure conditions: 1) without NO_x or UV exposure; 2) with NO_x but without UV exposure; and 3) with both NO_x and UV exposures. The samples subjected to Condition 3 were exposed to NO_x and UV for 5 h, plus one-hour stabilization time at beginning and another hour for re-stabilization time at the end (see Section 2.3 for detailed exposure arrangement). The samples subjected to Condition 2 were exposed to NO_x for a total of seven-hour period without UV (same period of NO_x exposure as Condition 3). These exposure conditions and arrangements were selected to examine the individual and combined effects of NO_x exposure, UV exposure, and TiO_2 doping. At the end of each experiment, the samples were removed from the reactor and subjected to chemical extraction and nitrite and nitrate measurements within 24 h.

Table 3
Summary on the test matrix, material composition, exposure conditions, and measured concentration of nitrogen in the forms of nitrite and nitrate.

Group ID[a]	OPC	5% TiO_2	Exposure Condition		Mass of Nitrogen (mg/kg)	
			NO_x	UV	Nitrite detection	Nitrate detection
PB	×				BDL	BDL
PB-N	×		×		2.77 ± 0.09	5.83 ± 0.55
PB-N-V	×		×	×	2.78 ± 0.02	5.66 ± 0.45
PT	×	×			BDL	BDL
PT-N	×	×	×		5.80 ± 0.22	8.08 ± 1.77
PT-N-V	×	×	×	×	16.99 ± 0.35	22.26 ± 3.25

[a] Sample ID: P – OPC, B – plain cement pastes without TiO_2, T- 5% TiO_2 inclusion, N – samples under NO_x exposure, and V – samples under UV radiation. For example, PT-N-V indicates TiO_2-doped OPC samples that are exposed to both NO_x gas and UV light; BDL: below detection limit.

2.5. Nitrite and nitrate measurements

The recovered samples were suspended in anoxic deionized (DI) water (purged by N_2 gas) in amber bottles to prevent further photo-induced reactions. Preliminary tests were conducted to determine the appropriate solid:liquid ratio (0.1 g in 10 to 100 mL), extraction time (4 h to 1 week), and solvent (DI water or KCl solution). A solid:liquid ratio of 0.1 g in 40 mL DI water, and 48 h reaction time were selected for all experiments. Varying these parameters to facilitate extraction – such as increasing dilution, increasing reaction time – produced no measurable increase in nitrite and nitrate concentration, demonstrating the suitability of this method for full extraction. After the extraction, the suspension was filtered through a 0.45 μm syringe filter. The pH of the filtrate was measured by pH test strips (EMD chemicals) and was found to be around 10. The filtrate was then analyzed for both nitrite and nitrate concentrations.

Nitrite concentration was determined using a colorimetric assay kit (Roche, Sigma Aldrich) and measured at 540 nm on a UV–vis spectrometer (Cary 60, Agilent). Nitrate concentration was determined using ion chromatography (IC, Dionex). The IC is equipped with an Ionpac® AS14A column (4 × 250 mm) combined with an Ionpac® AG14A guard column (4 × 50 mm), and a Dionex ED40 electrochemical detector. The mobile phase contained 8 mM Na_2CO_3 and 1 mM $NaHCO_3$, and the flow rate was 0.8 mL/min.

2.6. Examination of NO_x uptake and nitrite/nitrate formation

The nitrogen (N) mass of NO_x uptake (m_N) from the photodegradation test was compared with the total N mass from the nitrite (m_N') and nitrate (m_N'') measurements. The total amount of NO_x uptake throughout the photocatalytic process can be determined by Eqs. (9)–(11). For the purpose of comparison, the specific NO_x uptake (normalized by sample mass) is used in this study and with a unit of mg N per kg solid (denoted as mg/kg for simplicity).

$$Q_N = \frac{f}{V}\int_0^T (C_{[NO_x]uptake})dt \tag{9}$$

$$C_{[NO_x]uptake} = C_{[NO_x]in} - C_{[NO_x]out} \tag{10}$$

$$m_N = Q_N \times M_N \tag{11}$$

where Q_N = the amount of N uptake that is measured by NO_x analyzer (mol), $C_{[NO_x]_{uptake}}$ = uptake concentration of NO_x (ppb), $C_{[NO_x]_{in}}$ = inlet concentration of NO_x (ppb), $C_{[NO_x]_{out}}$ = outlet concentration of NO_x (ppb), t = time of NO_x absorption (min), T = the duration of the photocatalytic process (300 min), f = flow rate of NO_x at 23 °C and 1.01 kPa (L/min), V = 24.3 L (the volume of 1 mol ideal gas at 23 °C and 1.01 kPa), m_N = the mass of N uptake(mg/kg), and M_N = the molar mass of N = 14 g/mol.

The N mass from nitrite and nitrate measurements is determined by

Eqs. (12)–(15):

$$m_{NO_2^-} = C_{NO_2^-} \times DF \quad (12)$$

$$m_{NO_3^-} = C_{NO_3^-} \times DF \quad (13)$$

$$m_N' = m_{NO_2^-} \times \frac{M_N}{M_{NO_2^-}} \quad (14)$$

$$m_N'' = m_{NO_3^-} \times \frac{M_N}{M_{NO_3^-}} \quad (15)$$

where $m_{NO_2^-}$ = the mass of nitrite (mg/kg), $m_{NO_3^-}$ = the mass of nitrate (mg/kg), $C_{NO_2^-}$ = the concentration of nitrite measured by UV–vis (ppm), $C_{NO_2^-}$ = the concentration of nitrate measured by IC (ppm), DF = dilution factor used for wet chemical extraction (400 for all samples), m_N' = the mass of nitrogen from nitrite (mg/kg), m_N'' = the mass of nitrogen from nitrate (mg/kg), $M_{NO_2^-}$ = the molar mass of nitrite = 46 g/mol, and $M_{NO_3^-}$ = the molar mass of nitrate = 62 g/mol.

3. Results and discussion

3.1. Microstructure

The measured specific surface area (SSA) was 10.23 ± 0.98 m^2/g for the plain OPC samples (PB) and 16.90 ± 0.06 m^2/g for the TiO_2-doped OPC samples (PT) after 28 days of hydration. The SSA is increased by 65% due to the TiO_2 addition. The pore size distribution profiles of the PB and PT samples (Fig. 2) show larger amount of very small pores (< 5 nm) in Sample PT. The higher SSA and greater amount of micropores are attributed to the inclusion of TiO_2 nanoparticles, which possess intrinsically high SSA and ability to accelerate alite (C_3S) hydration due to nucleation and growth effects [45,46]. The surface area of C-S-H is in the range of 10s to 100s of m^2/g [47] and that of TiO_2 nanoparticles is larger than 225 m^2/g (Table 2). Therefore, while it is difficult to discern between the physical and chemical effects of nanoparticle addition, it is clear that TiO_2 addition leads to a higher SSA and larger amount of micropores in hydrated cementitious materials. The relationship between the microstructural property and NO_x uptake will be further discussed in Section 3.3.1.

3.2. Mass balance of NO_x uptake and nitrite/nitrate formation

The result of the NO_x photodegradation test during the UV-irradiation period for Sample PT-N-V (TiO_2-doped OPC exposed to both NO_x and UV) is shown in Fig. 3, where an instantaneous drop of NO_x concentration occurred upon UV illumination. This photodegradation of NO_x continued throughout the 5 h test period, but at a decreasing rate. This phenomenon agrees with findings by other researchers [10,12,21]. When the UV light was turned off, NO_x concentration returned to the initial value. The total N mass of NO_x uptake (m_N) is denoted by the shaded region in Fig. 3 and calculated to be 25.82 ± 0.57 mg/kg.

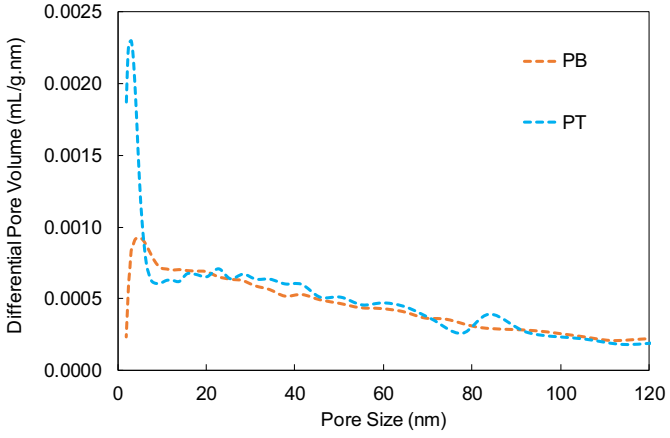

Fig. 2. Pore size distribution of plain OPC (PB) and 5% TiO_2-doped OPC (PT) samples.

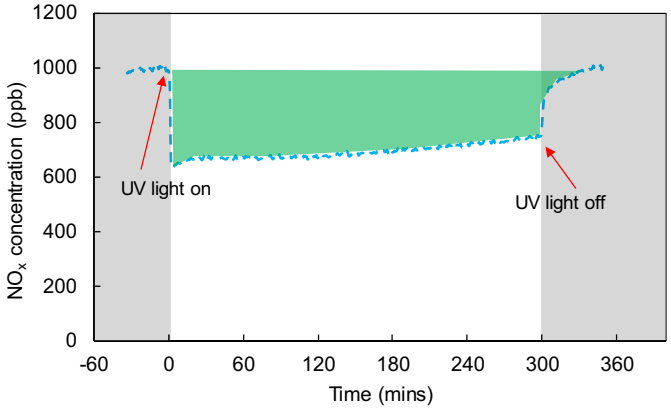

Fig. 3. Photodegradation of TiO_2-doped OPC sample (PT-N-V) that are exposed to both NO_x and UV light.

The N masses from nitrite and nitrate measurements are listed in Table 3. The N mass of nitrite and nitrate formation due to photocatalytic reactions can be estimated by the difference between Sample PT-N and PT-N-V. The N mass present in nitrite form (m_N') is 11.20 ± 0.42 mg/kg and in nitrate form (m_N'') is 14.18 ± 3.70 mg/kg. The total N mass in nitrite and nitrate combined ($m_N' + m_N''$) is 25.38 ± 3.73 mg/kg. Therefore, a mass balance is achieved with total N mass in NO_x uptake during the photocatalytic process falling within the margin of error for the total N mass presented in nitrite and nitrate ($m_N \cong m_N' + m_N''$).

3.3. NO_x uptake

The NO_x uptake by cement-based materials can be considered to occur via a two-step process: (1) the conversion of NO_x to nitrite and nitrate and (2) the binding of formed N species with cement paste. The difference in NO_x uptake is related to the differences in microstructural features (i.e. SSA and pore size distribution) and the photocatalytic activity induced by TiO_2 addition. These factors can be examined independently by comparing results among different sample groups.

3.3.1. Effect of microstructural features

For the plain OPC samples that are exposed to NO_x (PB-N and PB-N-V), both nitrite and nitrate are detected after exposure. As shown in Table 3, similar amounts of nitrite and nitrate are measured regardless of the presence of UV light. Therefore, the mechanism of converting NO_x to nitrite and nitrate by plain OPC is unlikely to be photocatalytic.

The mechanism of NO_x conversion to nitrite and nitrate should be related to heterogeneous catalytic reactions on the surface of hydrated cements. Researchers have demonstrated these reactions of NO_x on many different hydrated mineral surfaces [48–50]. For example, Grassian showed that NO_x reacts on the surface of hydrated SiO_2 particles (particles exposed to water overnight) but not on dehydrated SiO_2 particles (particles evacuated overnight) [48]. The detection of nitrite and nitrate in this study suggests that the complex surfaces of hydrated cementitious materials with their monolayers of water and pore-solution containing nanopores can also facilitate these heterogeneous catalytic reactions. Horgnies et al. [51] also observed decreased NO_x levels in the presence of conventional plain concrete and suggested that the high alkalinity in the cementitious environment also played an important role in NO_x conversion to nitrite and nitrate. Their proposed reactions with hydroxyls are as below:

$$NO + NO_2 + 2\,OH^- \rightarrow 2\,NO_2^- + H_2O \quad (16)$$

$$2\,NO_2 + 2\,OH^- \rightarrow NO_2^- + NO_3^- + H_2O \quad (17)$$

The previous studies also suggested that the heterogeneous surface catalytic reactions could be accelerated by high surface area, which relates to surface roughness, amount of micropores, and particle size [48–50]. This is also evidenced in this study by examining samples that are only exposed to NO_x (PB-N and PT-N), but with different SSA and amount of micropores. For Sample PT-N, the increase in NO_x uptake can be associated with the effect of TiO_2 addition on increased SSA and the amount of micropores with a size of < 5 nm (Section 3.1). Lee et al. [31] have also observed similar results indicating that a greater degree of NO_x degradation was achieved in TiO_2-doped cement pastes with a larger SSA. They have also suggested that the greater amount of micropores could also help hold more alkaline pore solution, which in turn could accommodate more nitrite and nitrate. Therefore, the NO_x uptake can be directly related to the microstructural features of cementitious materials.

Although the above studies have demonstrated the heterogeneous surface catalytic reactions in Sample PB-N and PT-N, none of them quantified the NO_x uptake. This information is critical to understand the intrinsic NO_x sequestration capability of cementitious materials and can be used it to remediate NO_x emissions resulting from their own production. This study quantifies the amount of NO_x uptake by measuring the concentration of nitrite and nitrate. The results are listed in Table 3. The concentration of both nitrite and nitrate in Sample PT-N increases compared to PB-N. The total N mass of NO_x uptake of PT-N is increased by 65% compared to PB-N. This increase coincides with the increase of SSA measured in Section 3.1. The increase in the nitrite is about 110% while the increase in the nitrate is about 30%. This difference leads to a change of the nitrite:nitrate concentration ratio from 1:2 in Sample PB-N to 1:1.3 in Sample PT-N. As discussed in Section 3.1, the higher SSA and greater amount of micropores in Sample PT-N induced by TiO_2 addition indicates a greater volume of C-S-H, in addition to the surface area and porosity intrinsic to the TiO_2 nanoparticles. Therefore, the increase of total NO_x uptake and larger increase of nitrite could be related to the increased amount of and more dispersed C-S-H and its different interaction with nitrite and nitrate. Again, the microstructural features, including SSA and pore size distribution, could be used as indicators to design cementitious materials for optimized NO_x uptake.

3.3.2. Effect of photocatalytic reactions

The total amount of NO_x uptake is increased by 360% in TiO_2-doped OPC that exposed to NO_x and UV light (PT-N-V) compare to the plain OPC samples (PB-N-V). The increased NO_x uptake is related to both the microstructural differences and the activation of photocatalytic activities induced by TiO_2 addition. The effects of microstructural features of cementitious materials on NO_x uptake have been discussed in the previous section.

The highest increase in NO_x uptake in Sample PT-N-V is mainly due to the photocatalytic activities (Eq. 1–8), which increase the conversion of NO_x to nitrite and nitrate ions and subsequently NO_x uptake. The relative amounts of nitrite and nitrate from the photocatalytic process alone (i.e., neglecting binding by the cementitious material itself) can also be determined by comparing Samples PT-N and PT-N-V. The results are provided in Table 3. Approximately half of the NO_x uptake is converted into nitrite during photocatalytic reactions, and the other half into nitrate. The higher NO_x uptake in Sample PT-N-V (360%) compared to Sample PT-N (65%) also indicates that the photocatalytic activity has a greater effect on NO_x uptake than the microstructural differences associated with TiO_2 introduction.

4. Conclusions

The NO_x uptake for both plain and TiO_2-doped OPC samples is compared in this study. Because NO_x is converted to nitrite and nitrate ions on the material surface, a combination of wet chemical extraction, UV–vis spectrophotometry and ion chromatography methods were used to quantify the concentrations of nitrite and nitrate that are bound within the hydrated cement paste. A mass balance is achieved between the total NO_x uptake and nitrite and nitrate formation. The effects of microstructural properties and photocatalytic reactions on NO_x uptake are examined. The conclusions are given below:

1. Similar NO_x uptake is observed in plain OPC samples (PB-N and PB-N-V) regardless of the presence of UV light, demonstrating that cement-based materials have the capacity for NO_x sequestration even in the absence of photocatalysts. By confirming the NO_x sequestration capability of plain OPC, policy makers can develop new strategies of remediating atmospheric NO_x by taking advantage of the NO_x sequestration capability of existing cement-based infrastructure, such as using it to remediate NO_x emissions resulting from their own production and construction.
2. The mechanism of NO_x conversion into nitrite and nitrate in samples that are only exposed to NO_x (PB-N and PT-N) is related to the surface catalytic reactions in cementitious environment. The addition of TiO_2 nanoparticles enhanced cement hydration and formation of C-S-H via nucleation and growth effects. The greater amount of C-S-H and the nano-TiO_2 addition contribute to the increase in SSA and the amount of < 5 nm micropores, and in turn increase the potential for NO_x uptake. The alkalinity in cementitious environment also plays an important role in NO_x conversion. With the TiO_2 addition, the concentration ratio between nitrite and nitrate changes from 1:2 to 1:1.3. This change is likely due to the larger amount of C-S-H in TiO_2–doped OPC samples. Therefore, the microstructural features, including SSA and pore size distribution, can be used as indicators for designing cementitious materials for optimized NO_x uptake.
3. For TiO_2-doped OPC samples that are exposed to both NO_x and UV (PT-N-V), the total NO_x uptake increases by 360%, compared to the plain OPC sample under the same exposure conditions (PB-N-V). The increase is attributed to the microstructure differences and activation of photocatalytic reactions induced by TiO_2 nanoparticles. By comparing the TiO_2-doped OPC samples with and without UV light exposure (PT-N-V vs PT-N), it can be concluded that the NO_x uptake is more greatly influenced by the photocatalytic activity than the microstructural changes associated with TiO_2 introduction.

Acknowledgements

This work is supported by the National Science Foundation under Grant No. CMMI-1362843. Any opinions, findings, and conclusions or recommendations expressed in this material are those of the author(s) and do not necessarily reflect the views of the National Science Foundation.

References

[1] R.M. Harrison Pollution, Causes, Effects and Control, 2 the Royal Society of Chemistry, Cambridge, (1992).
[2] The U.S. Environmental Protection Emission Standards for Electric Standards "United States Office of Air Quality Planning and Standards EPA-456/F-98-005", Protection Research Triangle Park, NC 27711, (September 1998).
[3] D. Elsom, Atmospheric Pollution, vol. 1, Basil Blackwell, New York, 1987.
[4] J.H. Seinfeld, Atmospheric Chemistry and Physics: From Air Pollution to Climate Change, vol. 1, Wiley, New York, 1998.
[5] Primary National Ambient air Quality Standards for Nitrogen Dioxide; Final Rule, 75 Fed. Reg. 26, (February 9, 2010) (to be codified at 40 C.F.R. pts. 50, 58).
[6] C.A. Latta, R.F. Weston, Methods for Reducing NOx Emissions, Plant Engineering, (1998) (September 1998).
[7] A. Fujishima, K. Honda, Electrochemical photolysis of water at a semiconductor electrode, Nature 238 (1972) 37–38.
[8] A. Fujishima, K. Hashimoto, T. Watanabe, TiO2 Photocatalysis: Fundamentals and Applications, BKC Inc, Tokyo, 1999.

[9] M.M. Ballari, Q.L. Yu, H.J.H. Brouwers, Experimental study of the NO and NO2 degradation by photocatalytically active concrete, Catal. Today 161 (2011) 175–180.

[10] R. Sugrañez, J.I. Alvarez, M. Cruz-Yusta, I. Marmol, J. Morales, J. Vila, L. Sanchez, Enhanced photocatalytic degradation of NOx gases by regulating the microstructure of mortar cement modified with titanium dioxide, Build. Environ. 69 (2013) 55–63.

[11] M.M. Ballari, H.J.H. Brouwers, Full scale demonstration of air-purifying pavement, J. Hazard. Mater. 254 (2013) 406–414.

[12] M.M. Hassan, H. Dylla, L.N. Mohammad, T. Rupnow, Evaluation of the durability of titanium dioxide photocatalyst coating for concrete pavement, Cons. Build. Mater. 24 (2010) 1456–1461.

[13] C.S. Poon, E. Cheung, NO removal efficiency of photocatalytic paving blocks prepared with recycled materials, Const. Build. Mater. 21 (2007) 1746–1753.

[14] A. Folli, S.B. Campbell, J.A. Anderson, D.E. Macphee, Role of TiO2 surface hydration on NO oxidation photo-activity, J. Photochem. Photobiol. A Chem. 220 (2011) 85–93.

[15] M. Montes, F.P. Getton, M.S.W. Vong, P.A. Sermon, Titania on silica. A comparison of sol-gel routes and traditional methods, J. Sol-Gel Sci. Technol. 8 (1997) 131–137.

[16] A.M. Ramirez, K. Demeestere, N. De Belie, T. Mäntylä, E. Levänen, Titanium dioxide coated cementitious materials for air purifying purposes: preparation, characterization and toluene removal potential, Build. Environ. 45 (2010) 832–838.

[17] J.S. Dalton, P.A. Janes, N.G. Jones, J.A. Nicholson, K.R. Hallam, G.C. Allen, Photocatalytic oxidation of NOx gases using TiO_2: a surface spectroscopic approach, Environ. Pollut. 120 (2002) 415–422.

[18] M.M. Ballari, M. Hunger, G. Hüsken, H.J.H. Brouwers, NOx photocatalytic degradation employing concrete pavement containing titanium dioxide, Appl. Catal. B Environ. 95 (2010) 245–254.

[19] R. Sugrañez, J.I. Álvarez, M. Cruz-Yusta, I. Mármol, J. Morales, J. Vila, L. Sánchez, Enhanced photocatalytic degradation of NOx gases by regulating the microstructure of mortar cement modified with titanium dioxide, Build. Environ. 69 (2013) 55–63.

[20] J. Chen, C.S. Poon, Photocatalytic cementitious materials: influence of the microstructure of cement paste on photocatalytic pollution degradation, Environ. Sci Technol. 43 (2009) 8948–8952.

[21] A. Yousefi, A. Allahverdi, P. Hejazi, Effective dispersion of nano-TiO2 powder for enhancement of photocatalytic properties in cement mixes, Constr. Build. Mater. 41 (2013) 224–230.

[22] Q.L. Yu, H.J.H. Brouwers, Indoor air purification using heterogeneous photocatalytic oxidation. Part I: experimental study, Appl. Catal. B Environ. 92 (2009) 454–461.

[23] M.Z. Guo, A. Maury-Ramirez, C.S. Poon, Photocatalytic activities of titanium dioxide incorporated architectural mortars: effects of weathering and activation light, Build. Environ. 94 (2015) 395–402.

[24] M. Pérez-Nicolás, J. Balbuena, M. Cruz-Yusta, L. Sánchez, I. Navarro-Blasco, J.M. Fernández, J.I. Alvarez, Cem. Con. Res. 70 (2015) 67–76.

[25] Baoguo Ma, Hainan Li, Xiangguo Li, Junpeng Mei, Yang Lv, Influence of nano-TiO_2 on physical and hydration characteristics of fly ash–cement systems, Constr. Build. Mater. 122 (2016) 242–253.

[26] J. Chen, C.S. Poon, Photocatalytic construction and building materials: from fundamentals to applications, Build. Environ. 44 (2009) 1899–1906.

[27] G. Hüsken, M. Hunger, H.J.H. Brouwers, Experimental study of photocatalytic concrete products for air purification, Build. Environ. 44 (2009) 2463–2474.

[28] D.E. Macphee, A. Folli, Photocatalytic concretes — the interface between photocatalysis and cement chemistry, Cem. Concr. Res. 85 (2016) 48–54.

[29] M.M. Ballari, Q.L. Yu, H.J.H. Brouwers, Experimental study of the NO and NO2 degradation by photocatalytically active concrete, Catal. Today 161 (1) (2011) 175–180.

[30] S. Devahasdin, C.J. Fan, K. Li, D.H. Chen, TiO2 photocatalytic oxidation of nitric oxide: transient behavior and reaction kinetics, J. Photochem. Photobiol. A Chem. 156 (2003) 161–170.

[31] B.Y. Lee, A.R. Jayapalan, M.H. Bergin, K.E. Kurtis, Photocatalytic cement exposed to nitrogen oxides: effect of oxidation and binding, Cem. Concr. Res. 60 (2014) 30–36.

[32] M. Balonis, M. Medala, F.P. Glasser, Influence of calcium nitrate and nitrite on the constitution of AFm and AFt cement hydrates, Adv. Cem. Res. 23 (3) (2011) 129–143.

[33] H. Justnes, Corrosion inhibitors for reinforced concrete, Corros. Reinf. Concr. Struct. (2005) 190–214.

[34] G. Falzone, M. Balonis, D. Bentz, S. Jones, G. Sant, Anion capture and exchange by functional coatings: new routes to mitigate steel corrosion in concrete infrastructure, Cem. Concr. Res. 101 (2017) 82–92.

[35] K.M. Miranda, M.G. Espey, D.A. Wink, A rapid, simple spectrophotometric method for simultaneous detection of nitrate and nitrite, Nitric Oxide 5 (1) (2001) 62–71.

[36] Q.H. Wang, L.J. Yu, Y. Liu, L. Lin, R.G. Lu, J.P. Zhu, Z.L. Lu, Methods for the detection and determination of nitrite and nitrate: a review, Talanta 165 (2017) 709–720.

[37] ASTM, Standard C114, "Standard Test Methods for Chemical Analysis of Hydraulic Cement", ASTM International, West Conshohocken, PA, 2013, https://doi.org/10.1520/C0114-13.

[38] S. Brunauer, P.H. Emmett, E. Teller, Adsorption of gases in multimolecular layers, J. Am. Chem. Soc. 60 (2) (1938) 309–319.

[39] E.P. Barrett, L.G. Joyner, P.P. Halenda, The determination of pore volume and area distributions in porous substances. I. Computations from nitrogen isotherms, J. Am. Chem. Soc. 73 (1) (1951) 373–380.

[40] M. Palacios, H. Kazemi-Kamyab, S. Mantellato, P. Bowen, Laser diffraction and gas adsorption techniques, in: K. Scrivener, R. Snellings, B. Lothenbach (Eds.), A Practical Guide to Microstructural Analysis of Cementitious Materials, CRC Press, 2015, pp. 445–484.

[41] I. Odler, The BET-specific surface area of hydrated Portland cement and related materials, Cem. Concr. Res. 33 (12) (2003) 2049–2056.

[42] M.C.G. Juenger, H.M. Jennings, The use of nitrogen adsorption to assess the microstructure of cement paste, Cem. Concr. Res. 31 (6) (2001) 883–892.

[43] ISO Fine Ceramics (Advanced Ceramics, Advanced Technical Ceramics) - Test Method for Air-Purification Performance of Semiconducting Photocatalytic Materials Part 1: Removal of Nitric Oxide, (2007).

[44] JIS R 1701-1 Fine Ceramics (Advanced Ceramics, Advanced Technical Ceramics) - Test Method for Air Purification Performance of Photocatalytic Materials-Part 1: Removal of Nitric Oxide, Japanese Standards Association, Tokyo, Japan, 2004.

[45] A. Jayapalan, B. Lee, S. Fredrich, K. Kurtis, Influence of additions of anatase TiO2 nanoparticles on early-age properties of cement-based materials, Transportation Research Record: Journal of the Transportation Research Board 2141 (2010) 41–46.

[46] B.Y. Lee, K.E. Kurtis, Influence of TiO_2 nanoparticles on early C3S hydration, J. Am. Ceram. Soc. 93 (10) (2010) 3399–3405.

[47] J.J. Thomas, H.M. Jennings, A.J. Allen, The surface area of cement paste as measured by neutron scattering: evidence for two C-S-H morphologies, Cem. Con. Res. 28 (6) (1998) 897–905.

[48] V.H. Grassian, Chemical reactions of nitrogen oxides on the surface of oxide, carbonate, soot, and mineral dust particles: implications for the chemical balance of the troposphere, J. Phys. Chem. A 106 (6) (2002) 860–877.

[49] A. Febo, C. Perrino, Prediction and experimental evidence for high air concentration of nitrous acid in indoor environments, Atmos. Environ. Part A 25 (5–6) (1991) 1055–1061.

[50] M.E. Jenkin, R.A. Cox, D.J. Williams, Laboratory studies of the kinetics of formation of nitrous acid from the thermal reaction of nitrogen dioxide and water vapour, Atmospheric Environment (1967) 22 (3) (1988) 487–498.

[51] M. Horgnies, I. Dubois-Brugger, E.M. Gartner, NOx de-pollution by hardened concrete and the influence of activated charcoal additions, Cem. Concr. Res. 42 (2012) 1348–1355.